Global Journal of Engineering and Technology Advances
eISSN: 2582-5003
Cross Ref DOI: 10.30574/gjeta
Journal homepage: https://gjeta.com/

(RESEARCH ARTICLE)

Check for updates

High cycle fatigue behavior of spot welds in DP 780, TRIP 780 and DC04 steel

Fabiano Ferreira Silva [1,*], Hermano Nascimento Junior [1], Roberto Rossy Chaves [1] and Marcello Rosa Dumont [2]

[1] *Materials Lab, Stellantis, Betim, Brazil.*
[2] *Department of Materials Engineering, Federal Center for Technological Education of Minas Gerais (CEFET-MG), Belo Horizonte, Brazil.*

Global Journal of Engineering and Technology Advances, 2023, 16(02), 266–279

Publication history: Received on 14 July 2023; revised on 24 August 2023; accepted on 26 August 2023

Article DOI: https://doi.org/10.30574/gjeta.2023.16.2.0173

Abstract

In this study, a methodology was successfully developed and validated to evaluate the behavior of spot welded joints of DP780, TRIP780 and DC04 steels in high cycle fatigue. Test specimens were made with three spot welds and Wohler curves were developed using the uniaxial tensile/traction load adopting the Owen R90C90 method. The spot welds showed an increase in fatigue life and a reduction in the maximum load, similar to steels. The influence of mechanical strength and material thickness tested and the types of fractures that occurred were compared. In low cycle regions, spot welds showed greater dispersion at maximum loading, between the different materials, and in higher cycle regions, this dispersion was reduced. The results obtained by adopting this method using three spot welds showed greater repeatability and less variation between the specimens of the same material. This developed method can be used with increased reliability to develop automotive bodies and spot welded components.

Keywords: Advanced High Strength Steels; Spot Welds; Fatigue; S-N Curve; Owen

1. Introduction

The body frame, also known as the Body-in-White, is one of the most important parts of a vehicle and normally contains thousands of spot welds. Failure of some of these welds and welded joints in the body frame can cause undesirable noise and vibrations and can lead to a reduction in the structure's crashworthiness. In addition, optimizing the number of spot welds, considering fatigue resistance, stiffness, among others, reduces production costs [1].

Several authors have researched spot welds and the combined effect of parameters such as material property and thickness, weld and notch geometry, fusion zone, microstructure and the loading condition on fatigue behavior [2].

There is not a vast body of literature on fatigue methodology to develop the S-N curve for components joined by spot welds, describing the test specimen definitions that best represent the application of spot welds and the way to treat the dispersion of the results. In this study, the spot weld behavior was evaluated when subjected to a high cycle fatigue test, the test parameterization was defined, its performance was evaluated and the S N curves were made using the Owen R90C90 method, through different types of AHSS (TRIP780, DP780) and IF (DC04). The manufacture of specimens with three aligned and equidistant spot welds, instead of a single central point, was defined and standardized. Adjustments were made to minimize dispersion in the fatigue results, as well as the influence of the test variables evaluated. Using the comparative study of spot welds between the AHSS, the behavior and influence of the material resistance compared to fatigue were observed. Concerning the IF steels, the behavior and influence of the increase in material thickness were evaluated. The types of fractures observed in the spot weld after the fatigue test in each test condition were described and compared.

* Corresponding author: Fabiano Ferreira Silva

Interstitial Free (IF) steels constitute one of the main groups of steels used in the manufacture of automotive parts, such as outer body panels, flooring, roofing and door frames, due to their excellent conformability, deep drawing capability, fatigue resistance, tensile strength and stiffness [3, 4, 5].

Dual Phase (DP) steels are one of the most used multiphase types among advanced high-strength steels (AHSS) in automotive parts. They are applied to automobile components, such as cross members, rails, wheels, bumper inner reinforcement and auto longeron. The microstructure of these steels consists of hard martensite islands in ferrite matrix. This dual-phase composite microstructure leads to a combination of high mechanical strength imparted by the martensitic phase and good ductility by the ferritic phase. This unique combination allows the use of thinner sheets, thus reducing vehicle weight, improving fuel efficiency, reducing greenhouse gas emissions and costs [6, 7].

Another class of AHSS widely used in the automotive industry is Transformation Induced Plasticity (TRIP) steel. Depending on their chemical composition and thermomechanical processing, the microstructure of these steels can consist of ferrite, bainite, martensite and retained austenite. The high fraction of ultrafine retained austenite obtained in these steels, due to the effect of strain hardening (transformation of austenite into martensite by plastic deformation), allows the manufacture of components with greater energy absorption during a collision [8, 9].

The relationship between the fatigue life of engineering materials and the applied stress is an important property for reliability in processes and designs. For safe-life design, fatigue test data is often presented in S-N curve form, for example, a log-log plot of stress S versus median fatigue life N, which is expressed in the number of cycles to failure. Fatigue life even under controlled stress levels and experimental conditions exhibits a large dispersion range. A conventional method to describe this curve and make the probability adjustment is to use approximately 15 specimens in each analyzed stress value, making it a time-consuming and expensive method [10].

2. Experimental Methodology

Commercial cold-rolled and annealed stress-relief steels DP780 and TRIP780 that were 1.2 mm thick and DC04 that was 0.7 mm and 1.2 mm thick were used. Rectangular specimens measuring 50 mm wide by 90 mm long were made. Spot welds among the test specimens were carried out with an overlap of 22 mm of material and with three aligned and equidistant spot welds, as shown in Figure 01.

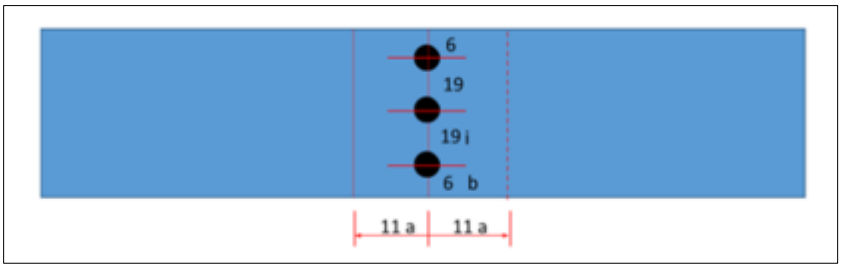

Figure 1 Dimensions and positioning of the test specimens and spot welds: (a) overlapping of the material, (b) distance between the edge of the plate and the spot weld, (i) distance between the spot welds. Measures in millimeters

The tensile tests on the steels were conducted, according to the ISO 6892-1: 2009 standard, in an INSTRON model 4467 universal testing machine, 30 kN load cell, video extensometer and Bluehill software, at room temperature.

The fatigue tests, on the welded specimens, were carried out using the INSTRON servo-hydraulic equipment, model 8801, with a frequency of 50 Hz, the loads were of the traction-traction type, sinusoidal curve, load ratio equal to R = 0,1 constant throughout the test. The S-N curves (in this study, the maximum load versus number of cycles to failure curve was used) were created with 5 stress levels, a minimum of 3 valid samples and a duration limited to 5.0 x 10^6 cycles or to fracture of the specimen. The calculations used, described in Equations 1 to 5, were [11, 12]:

$$\text{Maximum stress} = F_{máx} = \sigma . A_1 \quad \text{.....(1)}$$

$$\text{Minimum stress} = F_{mín} = F_{máx}.0{,}1 \quad \text{..... (2)}$$

$$\text{Mean stress} = F_m = \frac{F_{max} + F_{min}}{2} \quad \text{.....(3)}$$

$$\text{Alternating stress} = F_a = \frac{F_{max} - F_{min}}{2} \quad \text{.....(4)}$$

$$\text{Stress ratio: } R = \frac{F_{min.}}{F_{máx.}} \quad \text{.....(5)}$$

Where F_{max} is the maximum stress; σ is the tension; A_1 is the area; F_{min} is the minimum stress; F_m is the mean stress; F_a is the alternating stress; R = stress ratio.

To make the S-N curves, the fatigue parameters were obtained using the median and the Owen R90C90 method, obtained from the data of the tests carried out, and the slope factor of the S-N curve (k), the coefficient of fatigue resistance (σf ') and fatigue resistance exponent (b) [11, 13]. Basquin's equation was used, which defines the S-N curve, according to Equation 06 [11].

$$\sigma_a = \sigma_f'(2N_f)^b \quad \text{.....(06)}$$

Where σ_a is the true stress amplitude; σ_f' is the coefficient of fatigue resistance; $2N_f$ is the number of reversals; and b is the fatigue resistance exponent.

Equation 06 was converted into linear format, where fatigue life is the dependent variable as shown in Equations 07 to 09 [11, 14]:

$$\hat{Y} = \hat{A} + \hat{B}X \quad \text{.....(07)}$$

$$\hat{A} = \frac{-1}{b}\log(\sigma_f') \quad \text{.....(08)}$$

$$\hat{B} = \frac{1}{b} \quad \text{.....(09)}$$

Where $\hat{Y}$ is the fatigue life estimate; $\hat{A}$ is the regression coefficient estimate; $\hat{B}$ is the angular coefficient estimate; X is the variable; b is the fatigue resistance exponent; and σ_f' is the coefficient of fatigue resistance.

The linear regression used to solve $\hat{A}$ and $\hat{B}$, the fatigue properties, were calculated according to Equations 10 and 11 [11]:

$$\sigma_f' = 10^{\frac{-\hat{A}}{\hat{B}}} \quad \text{.....(10)}$$

$$b = \frac{1}{\hat{B}} \quad \text{.....(11)}$$

Parameters σ_f' and b represent the median S-N fatigue curve. The curve design represents the reliability and 90% confidence and was calculated using Owen's modified method [11].

When the curve was generated, the median S-N curve was shifted to the left by the product of sK_{Owen}. Parameter "s" is the parameter of the linear regression function and is defined, Equation 12, by [11, 13]:

$$s = \sqrt{\frac{1}{n_s - 2}\sum_{i=1}^{n_s}\left[Y_i - \left(\hat{A} - \hat{B}X_i\right)\right]^2} \quad \text{.....(12)}$$

Where s is the standard error of the sample and the number n_s is the number of samples used in the linear regression [11].

The morphological analysis of the fractured surfaces after the fatigue test was performed by scanning electron microscopy in Versa 3D DualBeam model equipment. Fractured regions in the spot weld nuggets and in the regions between the nuggets were analyzed.

3. Results and discussion

3.1. Microstructure

The results of the structures obtained in the metallography of DC04 steels that were 0.7 mm and 1.2 mm thick and DP780 and TRIP780 that were 1.2 mm thick are shown in Figure 02.

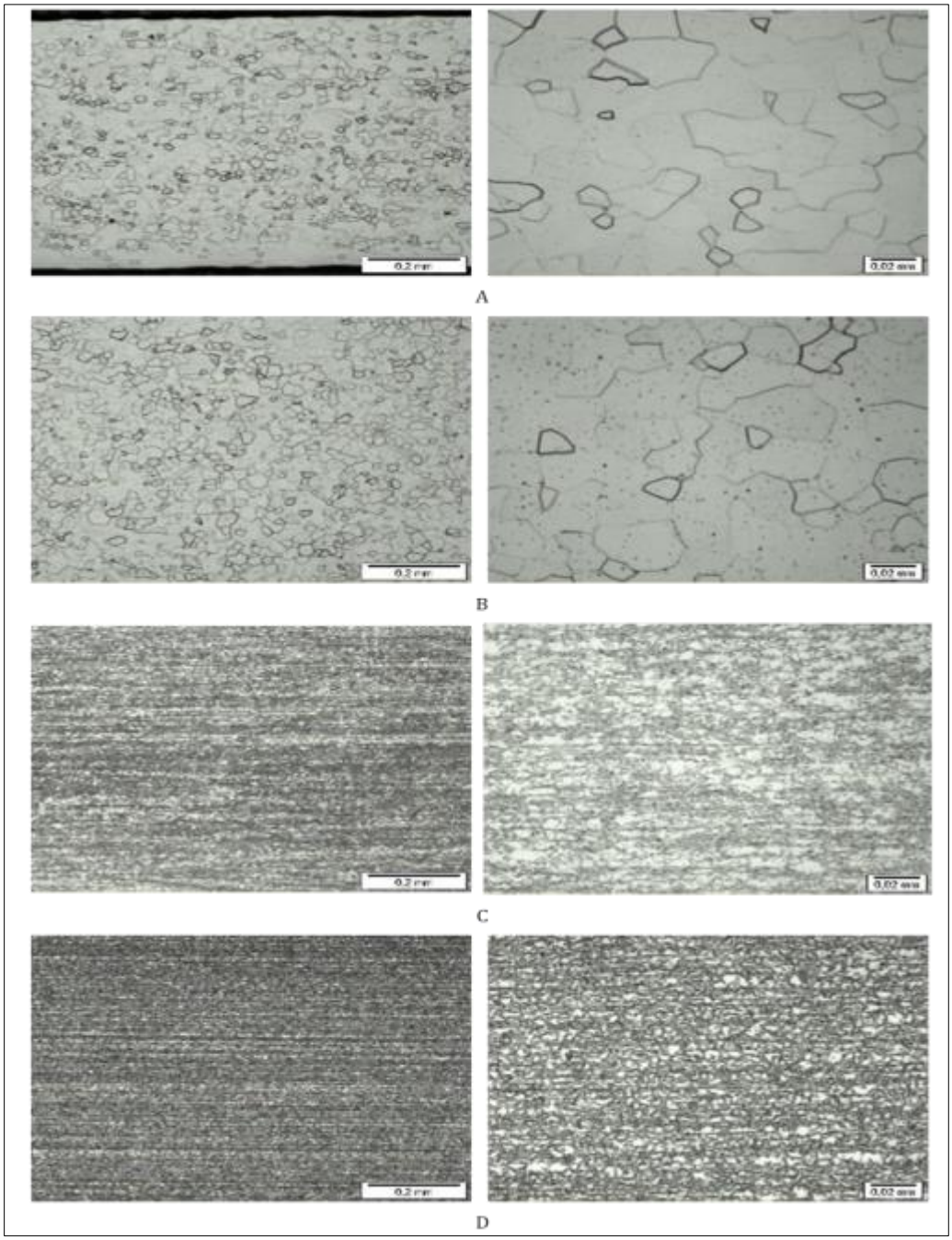

Figure 2 Microstructure of the steels analyzed at different magnifications: A) DC04 that was 0.7 mm thick; B) DC04 that was 1.2 mm thick; C) DP780 that was 1.2 mm thick and D) TRIP780 that was 1.2 mm thick

Both analyzed DC04 steels presented a grain size between 7 and 8, and the ferritic microstructure, according to the FCA MS.50002 standard [15]. Wei Li and Masomeh Oliaei, studied the IF steel and found the ferritic microstructure without any other phases, with the average grain size of 26.2 µm [16, 17], similar to that found in this study. The analyzed DP780 steel presented a microstructure consisting of ferrite and martensite, in addition to residual austenite, a result according to the FCA MS.50002 standard [15] and similar to the Ekrem Oztürk study [18]. The TRIP780 steel analyzed presented a microstructure consisting of ferrite, martensite, bainite and retained austenite, a result according to the FCA MS.50002 standard [15]. V. Paranthaman studied the TRIP780 steel and also found the microstructure composed of multiphase bainite, ferrite, retained austenite and martensite [19]. The microstructures of the analyzed steels are in accordance with their respective specifications.

3.2. Tensile test

Typical stress-strain curves were obtained for the analyzed materials DC04, TRIP780 and DP780 where all of them presented typical characteristics of ductile steels. The calculated results of tensile strength, yield strength, elongation, n, r and BH_2 and the values specified according to the standard are shown in Table 01.

Table 1 Results found in the tensile test of the analyzed samples

Material	Specified / sample	Tensile Strength (MPa)	Flow Limit (MPa)	Elongation (%)	R	N	BH_2 (MPa)
DC04	Spec.[a]	270 to 350	140 to 210	≥ 38	≥ 1.60	0.18	---
	0.7 mm	290	140	52	2.72	0.25	---
	1.2 mm	280	163	50	2.84	0.24	---
TRIP 780	Spec.[b]	≥ 780	470 to 600	21.00	≥ 0.16	---	---
	1.2 mm	888	494	21.43	0.22	---	---
DP780	Spec.[b]	≥ 780	450 to 560	≥ 14	---	---	≥ 30
	1,2 mm	843	504	14	---	---	83

[a] DIN EN 10130:2007 [20], [b] BS EN 10346:2009 [21]

All the analyzed materials presented values in the tensile tests as specified in the standard for the tested samples.

3.3. Fatigue Properties

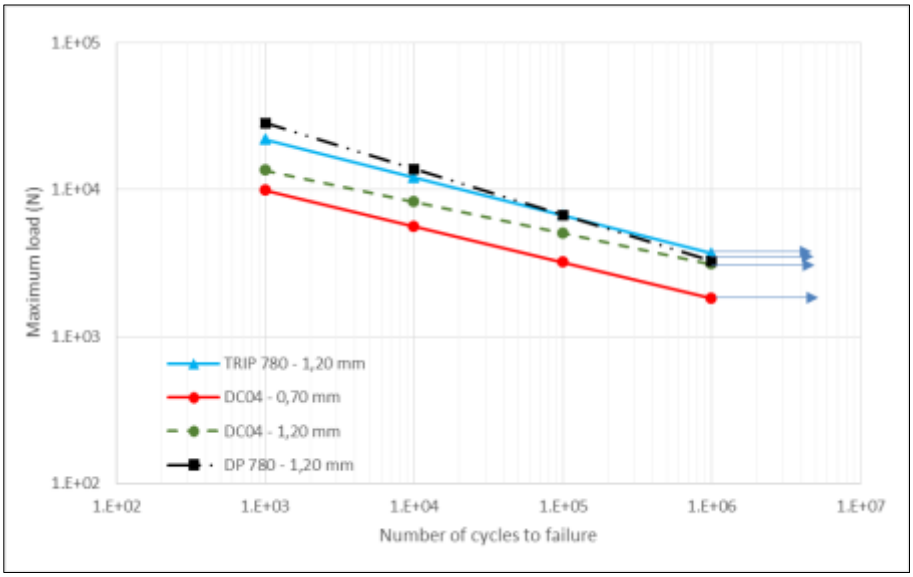

Figure 3 Maximum loads versus Number of cycles to failure obtained for welded test specimens of steels DC04, DP780 and TRIP780

The results of the maximum load versus number of cycles to failure curves of the welded specimens of DC04 steels that were 0.7 mm and 1.2 mm thick, as well as DP780 and TRIP780 that were 1.2 mm thick are shown in Figure 03. The visualization of stress curves versus number of cycles was used instead of the traditional curve of tension versus number of cycles. Using stress instead of tension was possible as the spot welds were performed in the same positions on all specimens and had parameters consistent with those used in automotive production processes. Thus, the area and its respective dispersion of the three spot welds, where the applied stress was equally distributed, was considered similar in all test specimens.

It was observed that the fatigue life of all welded samples increased as the maximum load reduced. This behavior is expected for metallic materials [22] showing that the welded bodies have fatigue characteristics consistent with their respective materials. The run-out data points for analyzed sample without failure were considered up to 1.0×10^6 cycles and are labeled with horizontal arrows in Figure 03. In addition, in low cycle regions, steel welds with higher mechanical resistance, TRIP780 and DP780, failed at higher maximum loads than the DC04. In the region of 1.0×10^3 cycles, dispersion of results of up to 1.8×10^4 N was observed for the different materials and thicknesses analyzed. In this region, the specimens DC04 0.7 mm and 1.2 mm presented load values close to 1.0×10^4 N and 1.4×10^4 N, respectively, TRIP780 presented load value of 2.2×10^4 N and DP780 presented load value of 2.8×10^4 N.

After increasing the number of cycles, a reduction in the dispersion of results was observed for welds performed on steels that were 1.2 mm thick, and in the range of 1.0×10^6 cycles, DC04, DP780 and TRIP780 presented similar values and close to 3.1×10^3 N, 3.3×10^3 N and 3.7×10^3 N, respectively. On the other hand, for the weld in DC04 material that was 0.7 mm thick, a value close to 1.8×10^3 N was observed.

The S-N curves of the steels in Figure 03 were compared with the results of other articles, but a similar study for a direct comparison of the results was not found in the literature. The articles reported using specimens with only one (01) spot weld. However, comparing with the values found in the steels analyzed and plotted in Figure 03, it can be observed that Kitae Kwon studied TRIP1180 steel that was 1.6 mm thick, and the S-N Curve found mean loading values of 74.03 % [23]. This value is expected because it is a material with higher mechanical strength and it is thicker. Heewon Cho studied TRIP980 steel that was 1.2 mm thick and the S-N Curve had mean values of 39.85% [24]. The value found was close to 33% (one third of the specimen with 03 spot welds). A higher value is expected because it is a material with a higher mechanical resistance value. H. Oikawa studied TRIP780 steel that was 1.2 mm thick and the results were with the welds with average values of 50.63% [25]. The values were well above 33% (one third of the specimen with 03 spot welds) which was expected because it is a material with the same resistance and thickness, observing that the author did not plot the S-N Curve. This showed better results than Heewon Cho [24], who studied TRIP980 steel that was 1.2 mm thick. Hamid Reza Ghanbari studied DP800 steel that was 1.8 mm thick and the results found welds with average values of 33.41% [26]. The values found were close to 33% (one third of the specimen with 03 spot welds). The value is lower than expected because it is a thicker material, observing that the author did not plot the S-N Curve. Trishita Ray studied DP780 steel with laser spot welds that were 1.0 mm thick and the results of the welds tested found mean values of 48.39% [2]. The values found were above 33% (one third of the specimen with 03 spot welds), but a different welding process was used. Sendong Ren studied DP980 steel that was 1.2 mm thick and the S-N Curve found average values of 60.30% [27]. The values found were much higher than 33% (one third of the specimen with 03 spot welds) because it is a material with a resistance class greater than that studied, and superior to the article by Hamid Reza Ghanbari [26], who studied DP800 steel that was 1.8 mm thick. Kaushal Kishore studied IF steel with DP600 steel that was 1.3 mm thick and the results found welds with mean values of 55.76% [28]. The values found above 33% (one third of the specimen with 03 spot welds) were expected as the material is thicker. Gorti Janardhan studied the IF steel with the HSNb steel that was 1.2 mm thick and the S-N Curve found mean values of 72.45% [29]. The values found were well above 33% (one third of the specimen with 03 spot welds) because the material is the same thickness and superior to the article by Kaushal Kishore [28], who studied IF steel with DP600 steel that was 1.3 mm thick. H. Oikawa studied IF steel that was 1.2 mm thick and the results were found with welds that had mean values of 43.46% [25]. The values found were above 33% (one third of the specimen with 03 spot welds). This value was expected as the material was the same thickness. It can be observed in the literature that there is no test standardization. Moreover, some researched articles did not make the S-N curve as they only plotted the results in graphs. There was a lack of linearity of the results and they were much higher than those expected compared to other articles, showing great dispersion between the results. There is a need for test standardization and 03 spot welds to carry out the fatigue test in the spot welds as using the methodology described here, it was possible to generate the S-N curves of 03 steels of different classes and of different thicknesses with consistent results compared with the articles studied, and the results found provide useful indications for fatigue test design in spot welds.

The results of the curves using the Owen method, the welds in DC04 steels that were 0.7 mm and 1.2 mm thik, and DP780 and TRIP780 that were 1.2 mm thick are shown in Figure 04.

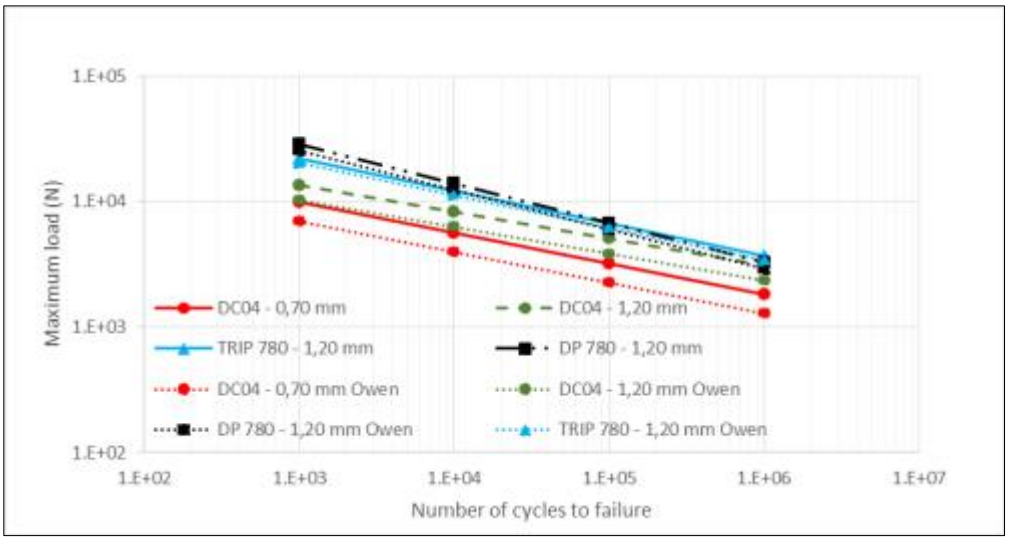

Figure 4 Owen R90C90 approach of Maximum load versus Number of cycles obtained for welded specimens of DC04, DP780 and TRIP780 steels

Adopting the Owen R90C90 method, the curves of the DP780 and TRIP780 steels were in the range of 1.0 x 10^3 cycles and the lines overlapped with the increase in the number of cycles. In the range of 3.0 x 10^5 cycles, the Owen curve of the DP780 steel was superimposed with the S-N curve of the DC04 material and was 1.2 mm thick. The Owen curve of the DC04 steel, which was 1.2 mm thick, overlapped the S-N curve of the DC04 steel, which was 0.7 mm thick in the range of 1.0 x 10^3 cycles and the curves distanced when the number of cycles was increased, at a range of 1.0 x 10^4 cycles. A greater dispersion was observed between the Owen R90C90 curves in relation to the S-N curves for the DC04 steels. This was due to the stress levels selected in the test, which had numbers lower than 1.0 x 10^3 cycles, therefore a high stress value. This difference increases the value of the standard error "s", calculation used in plotting the lines of the Owen R90C90 method, causing a greater displacement of the curves. For the finite fatigue life range, in which the stress amplitude shows a decreasing trend in relation to the number of cycles, the Owen method was able to model the uncertainty associated with the regression analysis [30]. Owen's method ensures that the data used in deriving the fatigue parameters are appropriate and indicative of the physical behavior of the material. The method allowed the precise derivation of the fatigue parameters, and thus the use of a fatigue software simulation to shorten the product development cycle, reducing the number of iterations in the design and test cycle [31].

3.4. Visual analysis of fractures

Visual analyses were carried out on the specimens with the lowest and highest number of cycles of steels DC04 that were 0.7 mm and 1.2 mm thick and DP780 and TRIP780 that were 1.2 mm thick to understand the crack propagation behavior, shown in Figure 05.

The low cycle specimens, DC04 0.7 mm and 1.2 mm Figure 05 (A and C) and TRIP780, Figure 05 (G), showed crack propagation only on the periphery of the nugget. The high cycle specimens, Figure 05 (B and D), the DP780 low and high cycle steel specimens, Figure 05 (E and F) and the high cycle TRIP780 steel specimens, Figure 05 (H) showed the crack propagation along the entire width of the specimen and parallel to the spot welds.

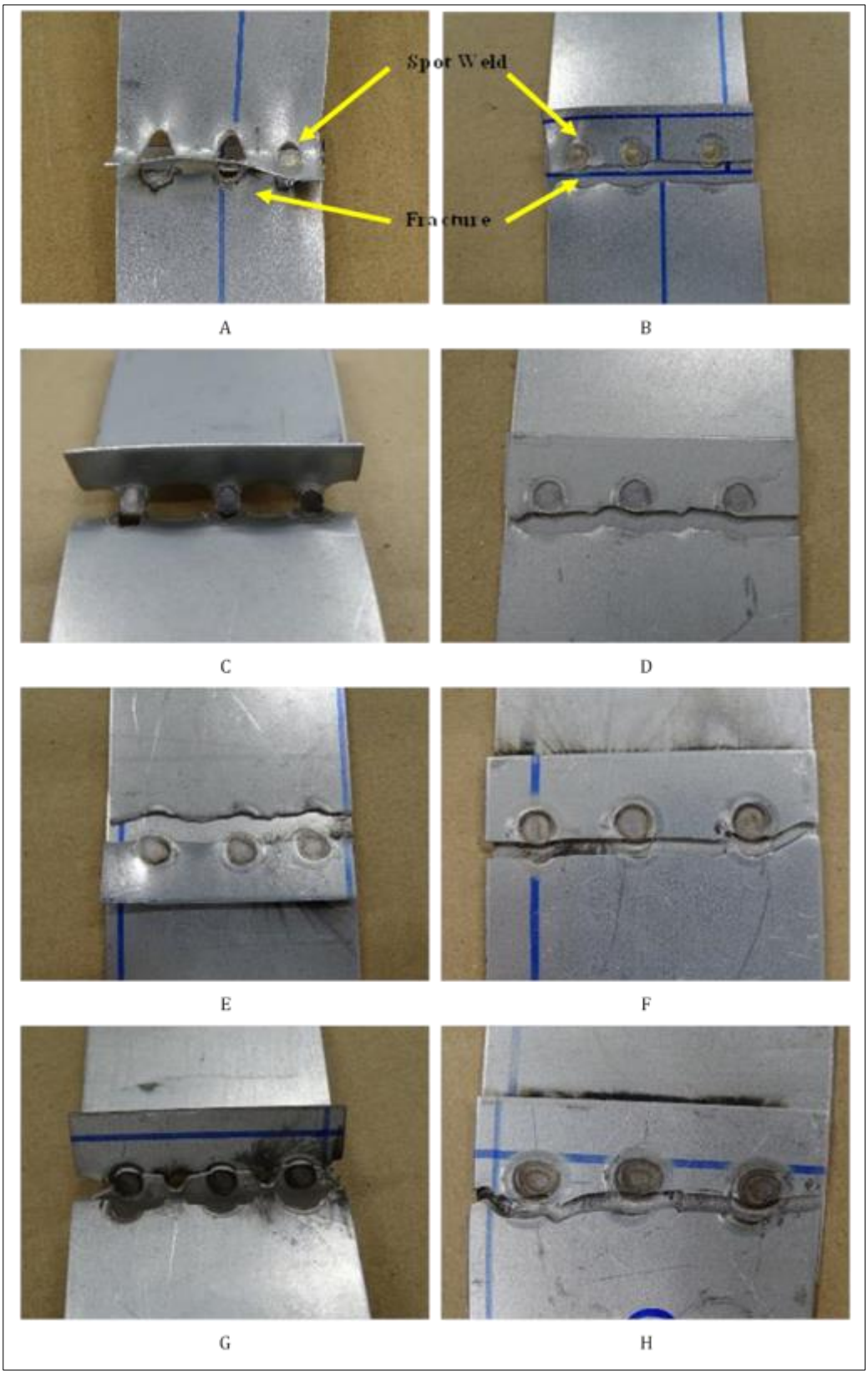

Figure 5 Fractures in the specimens in the analyzed IF and AHSS steels: A) DC04 that was 0.7 mm thick, 12.5 x 10^3 cycles; b) DC04 that was 0.7 mm thick, 1.0 x 10^6 cycles; C) DC04 that was 1.2 mm thick, 12.9 x 10^3 cycles; D) DC04 that was 1.2 mm thick, 6.3 x 10^5 cycles; E) DP780 12.1 x 10^3 cycles; F) DP780 1.5 x 10^6 c; G) TRIP780 8.6 x 10^3 cycles and H) TRIP780 1.1 x 10^6 cycles

3.5. Fractography of fatigue samples

The fracture morphologies, observed at SEM, of DC04 steel, which were 0.7 mm thick, the specimen with 12.5 x 10^3 cycles in the spot weld and the specimen with 1.0 x 10^6 cycles in the spot weld region and in the region between the spot welds are shown in Figure 06.

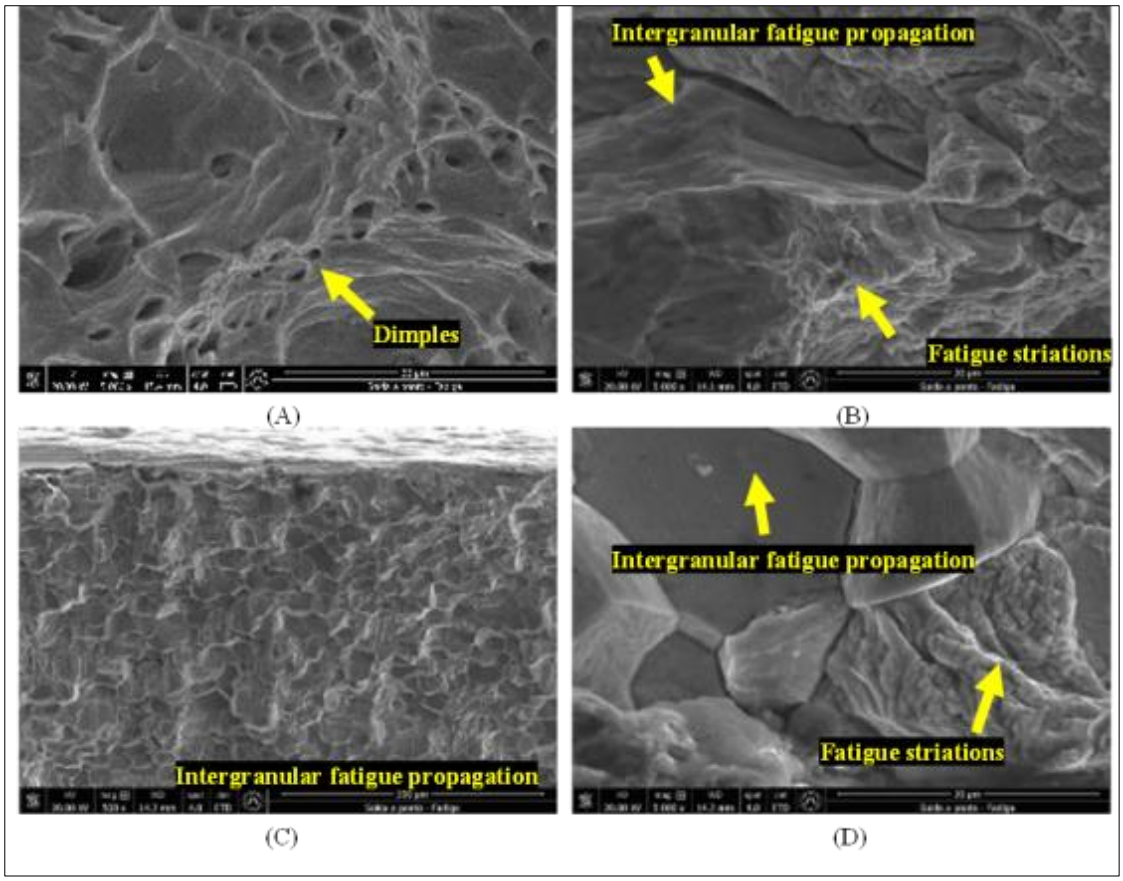

Figure 6 SEM image of fractures of DC04 steel specimens, which were 0.7 mm thick: a) spot weld region in the specimen with 12.5 x 10^3 cycles; b) spot weld region on the specimen with 1.0 x 10^6 cycles; c) and d) spot weld region on the specimen with 1.0 x 10^6 cycles and higher magnification image, respectively

Figure 06 (A) shows the fracture with a ductile region with micromechanisms essentially formed by dimples, typical morphology of a ductile fracture [32]. Figure 06 (B, C and D) illustrates typical fracture characteristics with fatigue striations and intergranular fatigue propagation, typical fatigue fracture morphology [33].

The DC04 steel fractures, which were 1.2 mm thick, the specimen with 12.9 x10^3 cycles, in the spot weld region and the specimen with 6.3 x 10^5 cycles in the spot weld region and in the region between the spot welds are shown in Figure 07.

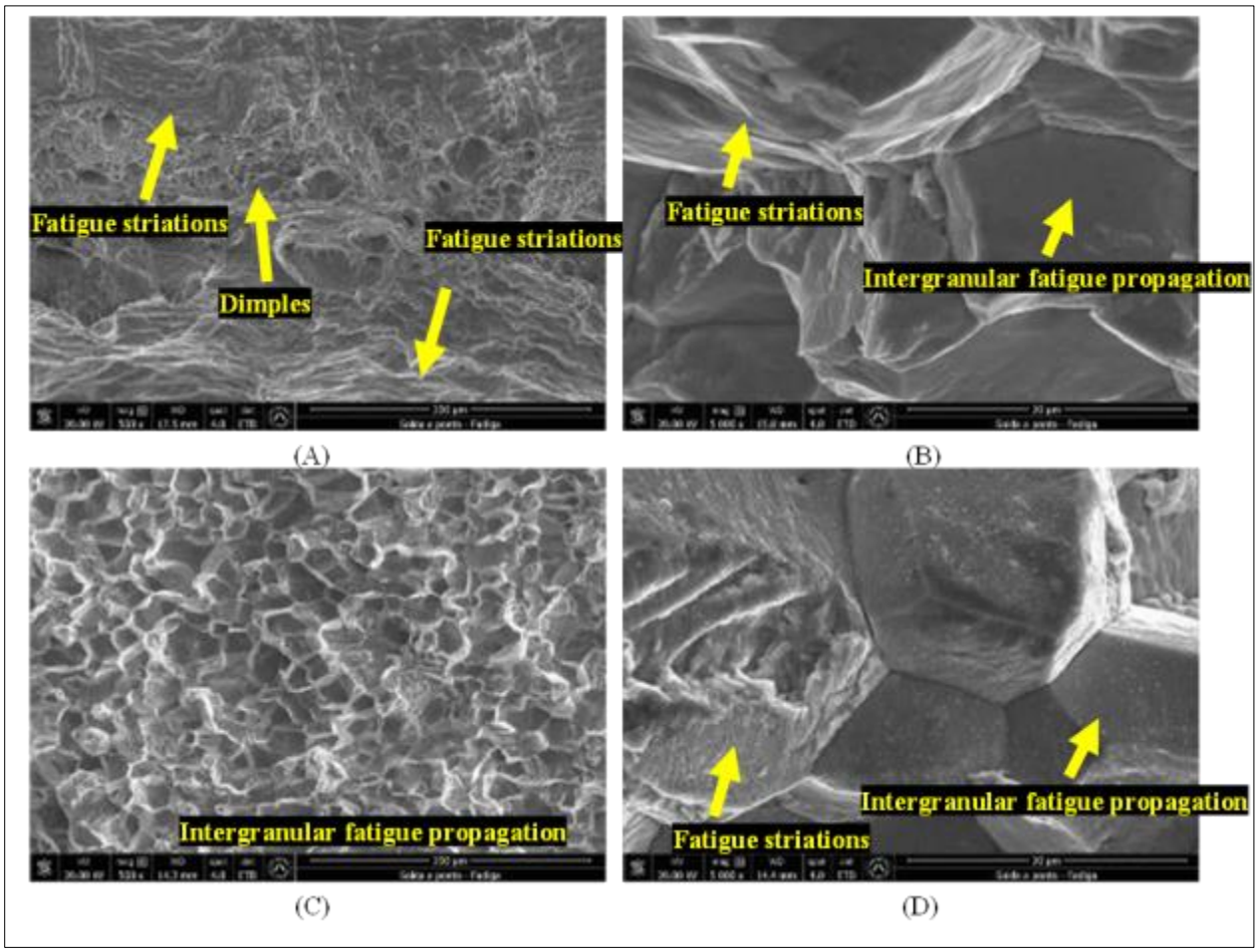

Figure 7 SEM image of fractures of DC04 steel specimens, which were 1.2 mm thick: a) spot weld region on the specimen with 12.9 x 10^3 cycles. b) spot weld region on the specimen with 6.3 x 10^5 cycles. c) and d) spot weld region on the specimen with 6.3 x 10^5 cycles and higher magnification image, respectively

Figure 07 (A) illustrates the fracture with mixed crack propagation, morphology and fatigue striation with stable crack propagation and micromechanisms formed by dimples referring to the region of unstable crack propagation. Fatigue fracture morphology and plastic deformation (overload). In Figure 07 (B, C and D), fractures with fatigue striations in the grain boundary and intergranular fatigue propagation are observed, typical fatigue fracture morphology. M. N. James [3] and V. Sajadifar [34] studied IF steels and verified that intergranular fatigue propagation during fatigue similar to the morphologies found in the steels analyzed in this work.

The fractures of the DP 780 steel, which were 1.2 mm thick, the specimen with 12.1 x 10^3 cycles and the specimen with 1.5 x 10^6 cycles in the spot weld region and in the spot weld region are show in Figure 08.

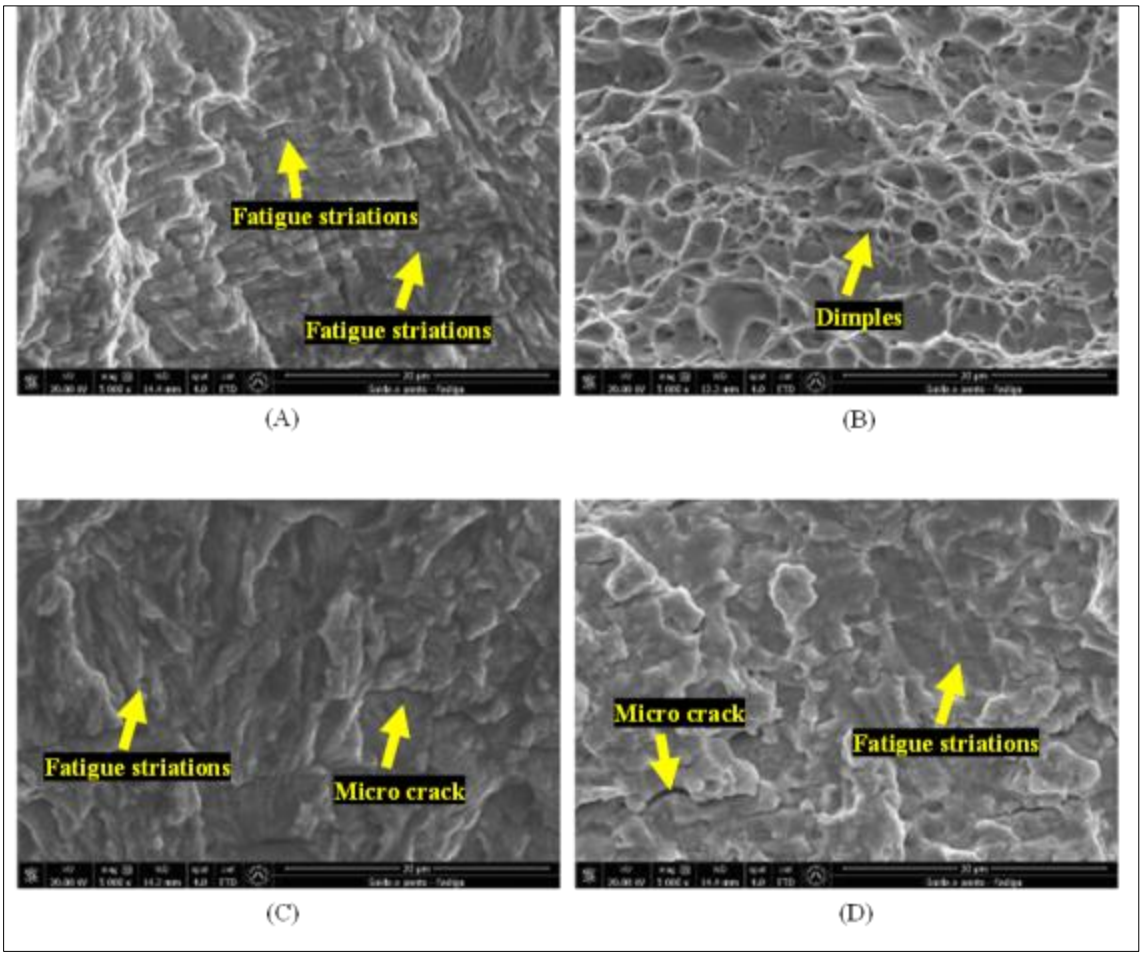

Figure 8 SEM image of fractures of the specimens of DP 780 steel, which is 1.2 mm thick: a) spot weld region on the specimen with 12.1 x 10^3 cycles; b) spot weld region with 12.1 x 10^3 cycles; c) spot weld region on the specimen with 1.5 x 10^6 cycles and d) spot weld region on the specimen with 1.5 x 10^6 cycles

Figure 08 (A, C and D) shows fracture morphologies with micromechanisms formed by fatigue striations and transgranular crack propagation, typical fatigue fracture morphology [35]. Figure 08 (B) shows a fracture with ductile morphology with micromechanisms formed essentially by dimples, a typical fracture structure with plastic deformation [36]. H. R. Ghanbari, studied DP steel and found fatigue striations and transgranular propagation [26] with morphology similar to that found in the analyzed DP780 steel in this paper.

Figure 09 shows the fractures of TRIP780 steel, which were 1.2 mm thick, the specimen with 8.6 x 10^3 cycles in spot weld region and the specimen with 1.1 x 10^6 cycles in the spot weld region and in the region between the spot welds.

Figure 09 (A) shows the fracture with micromechanisms formed by fatigue striations, dimples and the presence of microcracks. Figure 09 (B and C) illustrates fracture morphology with micromechanisms formed by fatigue striations and the presence of micro cracks. Both correspond to fatigue with transgranular crack propagation. Z. Zhang studied TRIP steel, and the micrograph analyzed by scanning electron microscopy after the fatigue test showed cracks with transgranular propagation, lamellar structure and a large amount of crack ramifications [37].

The analysis of the fractures of the test specimens with a lower number of cycles showed the influence of the material resistance, where the fractures presented fatigue with transgranular propagation, and micromechanisms typically formed by dimples, characteristic of deformation due to overload (plastic deformation of the material), where the material resistance has an influence on this type of deformation. The specimens with the highest number of cycles, DC04 steels, showed intergranular propagation and fatigue striations in the grain boundaries and the DP780 and TRIP780 steels showed fatigue striations and microcracks, typical fatigue fractures, where there was a reduction in the influence of the material resistance in this type of fracture.

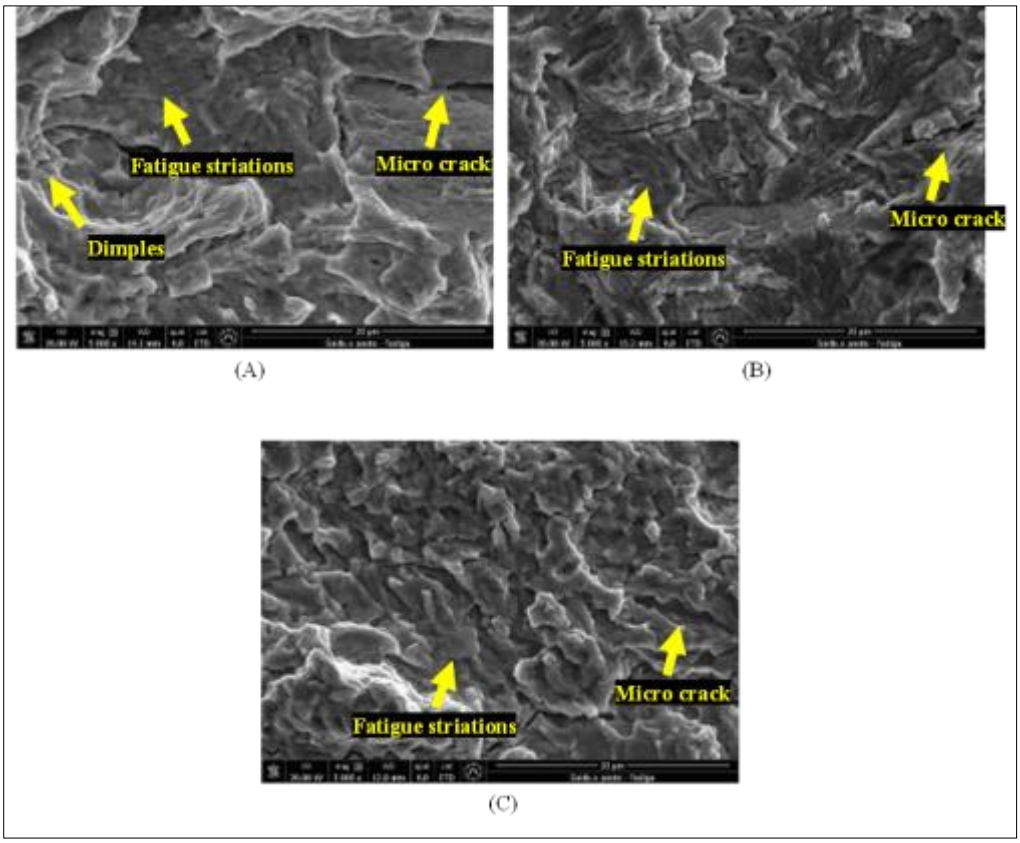

Figure 9 SEM image of fractures of TRIP780 steel specimens, which were 1.2 mm thick: a) spot weld region on the specimen with 8.6 x 10^3 cycles; b) spot weld region on the specimen with 1.1 x 10^6 cycles and c) spot weld region on the specimen with 1.1 x 10^6 cycles

4. Conclusion

Based on the test results carried out by the developed methodology, the high cycle fatigue behavior was observed in spot welds in the materials DP780, TRIP780 and DC04, using the S-N curves and the Owen method and the fracture mechanisms involved in the ruptures of the specimens using the scanning electron microscopy technique.

A reliable methodology was developed for the fatigue test in spot welds, using the specimen with 03 spot welds instead of 01 spot weld, to minimize the effect of the dispersion of the results. Using 03 spot welds on the test specimen, the results were repeatable, and the values obtained in the tests led to a smaller dispersion in the results. They were the closest condition to that used in the vehicle´s body frame.

Compliance with ethical standards

Acknowledgments

The authors are grateful for the technical support provided by Stellantis. This study was financed in part by the Coordination for the Improvement of Higher Education Personnel - Brazil (CAPES) - Finance Code 001.

Disclosure of conflict of interest

No conflict of interest to be disclosed.

References

[1] G. H. Farrahi, A. Ahmadi, and K. Reza Kasyzadeh, “Simulation of vehicle body spot weld failures due to fatigue by considering road roughness and vehicle velocity”, Simul Model Pract Theory, vol. 105, no August, p. 102168, 2020, doi: 10.1016/j.simpat.2020.102168.

[2] T. Ray, J. Kundu, A. Kundu, and M. Shome, “Fatigue behaviour of laser spot welds in dual phase 780 steel”, Int J Fatigue, vol. 132, mar. 2020, doi: 10.1016/j.ijfatigue.2019.105374.

[3] M. N. James, “Intergranular crack paths during fatigue in interstitial-free steels”, Eng Fract Mech, vol. 77, no 11, p. 1998–2007, jul. 2010, doi: 10.1016/j.engfracmech.2009.12.006.

[4] M. S. Kim et al., “Evolution of the microstructure and mechanical properties of interstitial-free steel during multi-axial diagonal forging”, Materials Science and Engineering A, vol. 846, jun. 2022, doi: 10.1016/j.msea.2022.143242.

[5] G. Janardhan, G. Mukhopadhyay, and K. Dutta, “Failure behaviour of Spot-welds on automotive steel sheets”, Mater Today Proc, vol. 62, no P10, p. 6120–6124, jan. 2022, doi: 10.1016/j.matpr.2022.05.020.

[6] H. Farivar, S. Richter, M. Hans, A. Schwedt, U. Prahl, and W. Bleck, “Experimental quantification of carbon gradients in martensite and its multi-scale effects in a DP steel”, Materials Science and Engineering A, vol. 718, no January, p. 250–259, 2018, doi: 10.1016/j.msea.2018.01.106.

[7] B. Das, A. Singh, K. S. Arora, M. Shome, e S. K. Paul, “Influence of pre-straining path on high cycle fatigue performance of DP 600 steel”, Int J Fatigue, vol. 126, no February, p. 369–380, 2019, doi: 10.1016/j.ijfatigue.2019.05.017.

[8] G. Park, K. Kim, S. Uhm, e C. Lee, “A comparison of cross-tension properties and fracture behavior between similar and dissimilar resistance spot-weldments in medium-Mn TRIP steel”, Materials Science and Engineering A, vol. 752, no January, p. 206–216, 2019, doi: 10.1016/j.msea.2019.03.023.

[9] I. Burda et al., “Fatigue crack propagation behavior of a micro-bainitic TRIP steel”, Materials Science and Engineering A, vol. 840, abr. 2022, doi: 10.1016/j.msea.2022.142898.

[10] J. Chen, S. Liu, W. Zhang, and Y. Liu, “Uncertainty quantification of fatigue S-N curves with sparse data using hierarchical Bayesian data augmentation”, Int J Fatigue, vol. 134, no December 2019, p. 105511, 2020, doi: 10.1016/j.ijfatigue.2020.105511.

[11] Y. L. Lee e D. Taylor, “Stress-Based Fatigue Analysis and Design”, em Fatigue Testing and Analysis, Y.-L. Lee, J. Pan, R. Hathaway, and M. Barkey, Orgs. Burlington: Elsevier Butterworth-Heinemann, 2005, p. 103–180. doi: 10.1016/B978-0-7506-7719-6.X5000-3.

[12] ISO 1099, Metallic materials — Fatigue testing — Axial force-controlled method, The International Organization for Standardization, Third edition, 2017.

[13] ISO 12107, Metallic materials - Fatigue testing - Statistical planning and analysis of data, The International Organization for Standardization, Second edition, 2012.

[14] ASTM, E739 - 10 Standard Practice for Statistical Analysis of Linear or Linearized Stress-Life (S-N) and Strain-Life (´ -N) Fatigue Data, ASTM International, vol. i, no Reapproved. 2010.

[15] MS.50002, SHEET STEEL FOR AUTOMOTIVE APPLICATION. FIAT CHRYSLER AUTOMOBILES, 2020.

[16] W. Li, M. Vittorietti, G. Jongbloed, and J. Sietsma, “The combined influence of grain size distribution and dislocation density on hardness of interstitial free steel”, J Mater Sci Technol, vol. 45, p. 35–43, maio 2020, doi: 10.1016/j.jmst.2019.11.025.

[17] M. Oliaei and R. Jamaati, “Improvement of the strength-ductility-toughness balance in interstitial-free steel by gradient microstructure”, Materials Science and Engineering A, vol. 845, jun. 2022, doi: 10.1016/j.msea.2022.143237.

[18] E. Öztürk and H. Arıkan, “Investigation of mechanical properties of laser welded dual-phase steels at macro and micro levels”, Opt Laser Technol, vol. 157, p. 108713, jan. 2023, doi: 10.1016/j.optlastec.2022.108713.

[19] V. Paranthaman, & K. S. Sundaram, e & L. Natrayan, “Effect of Silica Content on Mechanical and Microstructure Behaviour of Resistance Spot Welded Advanced Automotive TRIP Steels”, doi: 10.1007/s12633-021-01110-7/Published.

[20] D. I. fur Normung, EN 10130:2007-02 - Cold rolled low carbon steel flat products for cold forming - Technical delivery conditions, no February. Berlin, 2007.

[21] B. S. Instituion, BS EN 10346:2009 Continuously hot-dip coated steel flat products - Technical delivery conditions. 2009.

[22] S. M. A. K. Mohammed, Y. D. Jaya, A. Albedah, X. Q. Jiang, D. Y. Li, and D. L. Chen, "Ultrasonic spot welding of a clad 7075 aluminum alloy: Strength and fatigue life", Int J Fatigue, vol. 141, dez. 2020, doi: 10.1016/j.ijfatigue.2020.105869.

[23] K. Kwon, G. Jang, W. Kim, S. Uhm, T. Lee, and C. S. Lee, "Effect of type-C liquid metal embrittlement on mechanical properties of spot-welded TRIP steel", Journal of Materials Research and Technology, vol. 13, p. 2482–2490, jul. 2021, doi: 10.1016/j.jmrt.2021.06.041.

[24] H. Cho, S. Nam, I. Hwang, J. H. Oh, M. Kang, and Y. M. Kim, "Fatigue behaviors of resistance spot welds for 980 MPa grade TRIP steel", Metals (Basel), vol. 9, no 10, 2019, doi: 10.3390/met9101086.

[25] H. Oikawa, G. Murayama, S. Hiwatashi, K. Matsuyama, and M. Net, "RESISTANCE SPOT WELDABILITY OF HIGH STRENGTH STEEL SHEETS FOR AUTOMOBILES AND THE QUALITY ASSURANCE OF JOINTS Steel Corporation (Japan) 2 Forming Technologies R&D Center, Steel Research laboratories, Nippon Steel Corporation (Japan) 3 Smart Welding Technologies (United States)", 2007.

[26] H. R. Ghanbari, M. Shariati, E. Sanati, and R. Masoudi Nejad, "Effects of spot welded parameters on fatigue behavior of ferrite-martensite dual-phase steel and hybrid joints", Eng Fail Anal, vol. 134, abr. 2022, doi: 10.1016/j.engfailanal.2022.106079.

[27] S. Ren et al., "Post-weld cold working for fatigue strength improvement of resistance spot welded joint of advanced high-strength steel", J Mater Process Technol, vol. 299, jan. 2022, doi: 10.1016/j.jmatprotec.2021.117364.

[28] K. Kishore, P. Kumar, and G. Mukhopadhyay, "Microstructure, Tensile and Fatigue Behaviour of Resistance Spot Welded Zinc Coated Dual Phase and Interstitial Free Steel", Metals and Materials International, 2021, doi: 10.1007/s12540-020-00939-8.

[29] G. Janardhan, K. Kishore, G. Mukhopadhyay, and K. Dutta, "Fatigue Properties of Resistance Spot Welded Dissimilar Interstitial-Free and High Strength Micro-Alloyed Steel Sheets", Metals and Materials International, vol. 27, no 9, p. 3432–3448, set. 2021, doi: 10.1007/s12540-020-00678-w.

[30] A. Tridello et al., "Design against fatigue failures: Lower bound P-S-N curves estimation and influence of runout data", Int J Fatigue, vol. 162, set. 2022, doi: 10.1016/j.ijfatigue.2022.106934.

[31] C. R. Williams, Y. L. Lee, and J. T. Rilly, "A practical method for statistical analysis of strain-life fatigue data", Int J Fatigue, vol. 25, no 5, p. 427–436, 2003, doi: 10.1016/S0142-1123(02)00119-6.

[32] S. Yadav, A. Kamal, M. Sinha, and S. Ghosh, "Recrystallization in commercial grade interstitial-free steel, discussing criticality of martensite and massive ferrite nucleation along with mechanical property", Journal of Materials Research and Technology, vol. 15, p. 4750–4757, nov. 2021, doi: 10.1016/j.jmrt.2021.10.036.

[33] S. Mukherjee et al., "Insitu investigation of tensile deformation behaviour of cold-rolled interstitial-free high-strength steel in scanning electron microscope", Materials Science and Engineering A, vol. 776, mar. 2020, doi: 10.1016/j.msea.2020.139029.

[34] S. v. Sajadifar, T. Wegener, G. G. Yapici, and T. Niendorf, "Effect of grain size on the very high cycle fatigue behavior and notch sensitivity of titanium", Theoretical and Applied Fracture Mechanics, vol. 104, dez. 2019, doi: 10.1016/j.tafmec.2019.102362.

[35] M. Chinara, B. Jayabalan, B. Bhattacharya, A. Durga Prasad, S. Chatterjee, and S. Mukherjee, "Low cycle fatigue behaviour study of a nano precipitate strengthened ferrite-bainite 780 steel", Int J Fatigue, vol. 167, fev. 2023, doi: 10.1016/j.ijfatigue.2022.107294.

[36] S. Baek et al., "Effect of Mg remelting and mechanical hooks of steel on the mechanical and fatigue responses of resistance element welded AZ31/DP780 joints: Experimental, FEM and thermodynamic calculation studies", Journal of Materials Research and Technology, vol. 22, p. 1210–1237, jan. 2023, doi: 10.1016/j.jmrt.2022.11.157.

[37] Z. Zhang, M. Koyama, K. Tsuzaki, and H. Noguchi, "Three-dimensional characterization of low-cycle fatigue crack morphology in TRIP-maraging steel: Crack closure, geometrical uncertainty and wear", Int J Fatigue, vol. 143, fev. 2021, doi: 10.1016/j.ijfatigue.2020.106032.